Thermodynamic Properties of Model Solids with Short-Ranged Potentials from Monte Carlo Simulations and Perturbation Theory

A. Díez

Departamento de Física Aplicada, Universidad de Cantabria, E-39005 Santander, Spain

J. Largo

Dipartimento di Fisica, Universita di Roma La Sapienza, I-00185 Roma, Italy

J. R. Solana*

Departamento de Física Aplicada, Universidad de Cantabria, E-39005 Santander, Spain

Received: March 14, 2007; In Final Form: June 25, 2007

Monte Carlo simulations have been performed to determine the excess energy and the equation of state of fcc solids with Sutherland potentials for wide ranges of temperatures, densities, and effective potential ranges. The same quantities have been determined within a perturbative scheme by means of two procedures: (i) Monte Carlo simulations performed on the reference hard-sphere system and (ii) second-order Barker−Henderson perturbation theory. The aim was twofold: on the one hand, to test the capability of the "exact" MC-perturbation theory of reproducing the direct MC simulations and, on the other hand, the reliability of the Barker−Henderson perturbation theory, as compared with direct MC simulations and MC-perturbation theory, to determine the thermodynamic properties of these solids depending on temperature, density, and potential range. We have found that the simulation data for the excess energy obtained from the two procedures are in close agreement with each other. For the equation of state, the results from the MC-perturbation procedure also agree well with the direct MC simulations except for very low temperatures and extremely short-ranged potentials. Regarding the Barker−Henderson perturbation theory, we have found that in general the second-order approximation does not provide significant improvement over the first-order one.

I. Introduction

The Sutherland potential is of the form

$$u(r) = \begin{cases} \infty & r \le \sigma \\ -\epsilon\left(\frac{\sigma}{r}\right)^{\gamma} & r > \sigma \end{cases} \quad (1)$$

where parameters σ and $-\epsilon$ account for the diameter of the particles and the maximum potential depth, respectively, and the exponent γ determines the effective range of the potential, so that the higher is the value of γ the shorter is the effective range.

The shape of the potential function (eq 1) resembles the shape of other widely used potentials, such as the Lennard−Jones potential, for $\gamma = 6$, the Girifalco potential for C_{60}, for $\gamma \approx 12$,[1] and the Mie potential, widely used to describe pure fluids and solutions as well as solids, for a wide range of values of γ depending on the real system to be modeled.[2] The advantage of a potential of the form of eq 1 with respect to these others is that in the former, the diameter of the particles is well defined. The simple mathematical form of the potential (eq 1), together with its flexibility to reproduce a wide variety of intermolecular interactions, has led recently to a number of applications for modeling interactions in complex fluids[3,4] and nanocomposite materials.[5]

The Sutherland potential has shown to be useful too for phase equilibria calculations. Thus, this model potential was used successfully within the framework of the SAFT-VR approach to obtain the liquid−vapor coexistence properties of chain-molecular fluids.[6,7] The same potential with $\gamma = 8$ allowed one to determine the phase diagram of microgel dispersions in good agreement with experiment.[8] Very recently, this potential with $\gamma = 6$ has been shown to be appropriate for vapor−liquid equilibria calculations for C_{60} fullerenes.[9]

In this situation, one might reasonably expect this kind of system would have been extensively studied both from theory and from computer simulation. However, computer simulations on this system have been scarcely reported. For the fluid, quite extensive simulation data for the excess energy and the compressibility factor have been reported in ref 10 and more recently in ref 11 for several values of γ and a wide range of densities and temperatures, particularly in the latter reference. Simulation data on the radial distribution function for the high-density fluid may be found in ref 12 for several temperatures and effective ranges of the potential. Simulation data for liquid−vapor coexistence densities and critical parameters for several values of γ were reported in ref 13 and triple point parameters in ref 14.

In regard to theory, the amount of research devoted to this kind of fluid is equally scarce,[11,12,15−17] although recently we reported[11] a quite complete analysis of the performance of the Barker−Henderson perturbation theory[18,19] for the thermodynamic properties of this kind of fluid, and still more recently[12]

* Author to whom correspondence should be addressed. E-mail: ramon.solana@unican.es.

10.1021/jp072059z CCC: $37.00
Published on Web 08/07/2007

TABLE 1: Simulation Data for $\gamma = 6$[a]

ρ^*	0.90	0.95	1.00	1.05	1.10	1.15	1.20	1.25	1.30
$T^* = 0.2$									
Z[b]	−4.92(5)						−26.67(3)	−26.15(3)	−20.43(3)
$U^E/N\epsilon$[b]	−4.45(2)	−4.97(5)	−5.1(1)	−5.1(5)			−5.225	−5.618	−6.042
$T^* = 0.4$									
Z	−1.03(2)	−0.52(3)	−0.95(5)	−4.95(2)	−5.49(2)	−5.19(2)	−3.89(2)	−0.44(2)	8.08(3)
$U^E/N\epsilon$	−3.468(1)	−3.712(1)	−4.016(2)	−4.178	−4.493	−4.840	−5.213	−5.614	−6.041
$T^* = 0.6$									
Z	2.70(2)	3.75(3)	0.53(2)	0.28(2)	0.70(2)	1.66(2)	3.84(2)	8.05(3)	17.41(4)
$U^E/N\epsilon$	−3.382	−3.651	−3.852	−4.149	−4.479	−4.832	−5.208	−5.610	−6.036
$T^* = 0.8$									
Z	4.59(2)	5.96(3)	2.84(2)	3.04(2)	3.75(2)	5.22(2)	7.71(2)	12.42(3)	22.24(4)
$U^E/N\epsilon$	−3.351	−3.630	−3.835	−4.141	−4.473	−4.829	−5.207	−5.609	−6.036
$T^* = 1.0$									
Z	5.85(2)	7.22(2)	4.32(2)	4.72(2)	5.65(2)	7.29(2)	10.05(2)	15.01(3)	25.04(4)
$U^E/N\epsilon$	−3.336	−3.616	−3.826	−4.136	−4.470	−4.827	−5.206	−5.609	−6.036
$T^* = 1.5$									
Z	7.481(2)	9.04(2)	6.23(2)	6.95(2)	8.16(2)	10.07(2)	13.15(2)	18.49(2)	28.91(4)
$U^E/N\epsilon$	−3.319	−3.602	−3.815	−4.129	−4.466	−4.825	−5.205	−5.609	−6.036
$T^* = 2.0$									
Z	8.277(2)	9.77(6)	7.24(2)	8.06(2)	9.41(2)	11.50(2)	14.73(2)	20.21(2)	30.79(4)
$U^E/N\epsilon$	−3.310	−3.593(1)	−3.810	−4.126	−4.464	−4.824	−5.204	−5.609	−6.036
$T^* = 3.0$									
Z	9.12(2)	8.18(4)	8.23(1)	9.21(2)	10.74(2)	12.92(2)	16.29(2)	21.92(2)	32.71(4)
$U^E/N\epsilon$	−3.303	−3.529(1)	−3.805	−4.123	−4.463	−4.823	−5.204	−5.608	−6.036

[a] Corrections due to the truncation of the potential have not been included. The number between parentheses indicates the error in the last significant digit of the compressibility factor. For the excess energy, the statistical error in most cases is beyond the third decimal place and when this is the case, it is not indicated. [b] Averages over several independent runs.

TABLE 2: Simulation Data for $\gamma = 12$[a]

ρ^*	0.90	0.95	1.00	1.05	1.10	1.15	1.20	1.25	1.30
$T^* = 0.2$									
Z[b]	−3.3(3)	−3.3(2)	−4.0(4)						−39.04(6)
$U^E/N\epsilon$[b]	−3.10(8)	−3.31(8)	−3.60(9)	−3.79(5)	−3.94(2)	−4.25(9)	−4.3(1)	−4.52(4)	−4.455
$T^* = 0.4$									
Z	1.78(4)	2.42(3)	2.15(5)	1.04(5)	−2.56(3)	−4.31(4)	−5.56(3)	−5.67(3)	−1.67(4)
$U^E/N\epsilon$	−2.192(1)	−2.376(1)	−2.664(2)	−3.267(2)	−2.881(2)	−3.134	−3.478	−3.911	−4.442
$T^* = 0.6$									
Z	4.54(3)	5.61(3)	5.98(9)	2.52(2)	2.03(3)	1.86(3)	2.36(3)	4.43(3)	10.884(4)
$U^E/N\epsilon$	−2.018(1)	−2.221(1)	−2.432(2)	−2.510	−2.760	−3.068	−3.442	−3.892	−4.429
$T^* = 0.8$									
Z	6.06(2)	7.44(3)	5.03(3)	4.61(2)	4.68(2)	5.21(2)	6.54(3)	9.64(3)	17.28(4)
$U^E/N\epsilon$	−1.951(1)	−2.167(1)	−2.247(1)	−2.458	−2.724	−3.046	−3.430	−3.886	−4.428
$T^* = 1.0$									
Z	7.04(2)	8.36(3)	5.87(2)	5.97(2)	6.40(2)	7.31(2)	9.13(3)	12.77(3)	21.195(4)
$U^E/N\epsilon$	−1.919(1)	−2.130(1)	−2.205(1)	−2.431	−2.707	−3.035	−3.423	−3.883	−4.427
$T^* = 1.5$									
Z	8.26(2)	9.88(2)	7.23(2)	7.66(2)	8.61(2)	10.09(2)	12.49(2)	16.96(3)	26.23(4)
$U^E/N\epsilon$	−1.873(1)	−2.089	−2.159	−2.396	−2.683	−3.019	−3.414	−3.880	−4.426
$T^* = 2.0$									
Z	8.86(2)	10.59(2)	7.96(2)	8.60(2)	9.72(2)	11.49(2)	14.17(2)	19.10(3)	28.76(4)
$U^E/N\epsilon$	−1.851	−2.070	−2.139	−2.381	−2.671	−3.011	−3.409	−3.878	−4.426
$T^* = 3.0$									
Z	9.46(2)	10.5(1)	8.71(2)	9.53(2)	10.95(2)	12.89(2)	15.93(2)	21.18(3)	31.36(4)
$U^E/N\epsilon$	−1.829	−2.014	−2.119	−2.366	−2.661	−3.004	−3.406	−3.876	−4.425

[a] Corrections due to the truncation of the potential have not been included. The number between parentheses indicates the error in the last significant digit of the compressibility factor. For the excess energy, the statistical error in most cases is beyond the third decimal place and when this is the case, it is not indicated. [b] Averages over several independent runs.

we performed a similar analysis using the first-order mean spherical approximation.[20,21]

In contrast with fluids, crystalline solids interacting by means of model potentials have been much less frequently studied, with the possible exception of the hard-sphere solid, and to the best of our knowledge, the behavior of solids with Sutherland potentials has not been studied before from theory nor computer simulation. This is the aim of this paper, for which we have performed extensive computer simulations for the thermodynamic properties of Sutherland fcc solids for several values of γ, temperatures, and densities. These are described in the next section. Section III summarizes the foundations of two versions

TABLE 3: Simulation Data for $\gamma = 18$[a]

ρ^*	0.90	0.95	1.00	1.05	1.10	1.15	1.20	1.25	1.30
$T^* = 0.2$									
Z[b]	−2.5(1)	−2.9(1)	−3.5(1)					−11.3(7)	−15.8(4)
$U^E/N\epsilon$[b]	−2.70(3)	−2.80(2)	−3.00(3)	−3.38(5)	−3.66(2)	−3.82(2)	−3.94(4)	−4.21(1)	−4.48(1)
$T^* = 0.4$									
Z	3.03(4)	3.75(4)	4.47(6)	2.91(6)	2.6(1)	−1.86(4)	−4.55(4)	−7.29(5)	−8.21(4)
$U^E/N\epsilon$	−1.817(2)	−1.984(1)	−2.179(2)	−2.578(3)	−3.13(3)	−2.632(2)	−2.897(1)	−3.289	−3.852
$T^* = 0.6$									
Z	5.411(3)	6.40(3)	6.83(7)	4.17(3)	3.48(4)	3.02(3)	2.68(3)	2.89(4)	6.48(5)
$U^E/N\epsilon$	−1.604(1)	−1.778(2)	−1.945(3)	−1.995(2)	−2.191(1)	−2.454(1)	−2.790	−3.231	−3.822
$T^* = 0.8$									
Z	6.73(2)	8.04(3)	6.81(3)	5.80(2)	5.77(3)	5.95(3)	6.65(3)	8.43(4)	13.85(6)
$U^E/N\epsilon$	−1.511(1)	−1.695(1)	−1.778(2)	−1.898(1)	−2.116(1)	−2.396	−2.754	−3.214	−3.817
$T^* = 1.0$									
Z	7.58(2)	8.96(2)	6.81(3)	6.88(2)	7.20(3)	7.85(3)	9.09(3)	11.74(4)	18.23(4)
$U^E/N\epsilon$	−1.465(1)	−1.647(1)	−1.673(1)	−1.849(1)	−2.078	−2.368	−2.734	−3.204	−3.813
$T^* = 1.5$									
Z	8.63(2)	10.25(2)	7.96(2)	8.33(2)	9.15(2)	10.42(2)	12.45(3)	16.23(3)	24.36(4)
$U^E/N\epsilon$	−1.402(1)	−1.587(1)	−1.603(1)	−1.787	−2.029	−2.331	−2.710	−3.191	−3.809
$T^* = 2.0$									
Z	9.22(2)	10.82(2)	8.46(2)	9.11(2)	10.20(2)	11.71(2)	14.16(2)	18.51(3)	27.37(3)
$U^E/N\epsilon$	−1.376(1)	−1.558	−1.565(1)	−1.759	−2.006	−2.313	−2.698	−3.186	−3.807
$T^* = 3.0$									
Z	9.73(2)	11.58(2)	9.03(2)	9.86(2)	11.20(2)	13.09(2)	15.89(2)	20.77(3)	30.41(3)
$U^E/N\epsilon$	−1.347(1)	−1.536	−1.533	−1.732	−1.984	−2.297	−2.687	−3.180	−3.805

[a] Corrections due to the truncation of the potential have not been included. The number between parentheses indicates the error in the last significant digit of the compressibility factor. For the excess energy, the statistical error in most cases is beyond the third decimal place and when this is the case, it is not indicated. [b] Averages over several independent runs.

TABLE 4: Simulation Data for $\gamma = 36$[a]

ρ^*	0.90	0.95	1.00	1.05	1.10	1.15	1.20	1.25	1.30
$T^* = 0.2$									
Z[b]						−5.9(2)	−7.7(2)	−11.3(7)	−17.7(6)
$U^E/N\epsilon$[b]	−2.21(3)	−2.32(3)	−2.46(2)	−2.54(1)	−2.86(3)	−2.95(1)	−3.29(6)	−3.76(4)	−3.97(1)
$T^* = 0.4$									
Z	5.06(7)	5.96(7)	6.97(8)	5.9(1)	4.29(8)	3.16(9)	1.12(8)	−2.17(8)	−8.39(9)
$U^E/N\epsilon$	−1.318(2)	−1.475(1)	−1.629(2)	−1.749(7)	−1.851(5)	−1.966(2)	−2.179(2)	−2.489(2)	−2.903(1)
$T^* = 0.6$									
Z	6.17(2)	7.20(2)	7.24(6)	5.95(3)	5.86(3)	5.79(3)	5.47(3)	4.88(4)	4.11(6)
$U^E/N\epsilon$	−1.061(2)	−1.194(1)	−1.284(5)	−1.319(2)	−1.460(2)	−1.648(2)	−1.890(1)	−2.233(1)	−2.753
$T^* = 0.8$									
Z	7.58(2)	8.89(3)	7.72(4)	7.61(3)	8.00(3)	8.47(3)	9.03(3)	9.91(5)	12.05(6)
$U^E/N\epsilon$	−0.960(1)	−1.097(1)	−1.100(2)	−1.192(2)	−1.341(1)	−1.536(1)	−1.794(1)	−2.160	−2.716
$T^* = 1.0$									
Z	8.42(2)	9.80(2)	8.11(2)	8.53(2)	9.07(3)	9.95(3)	11.07(3)	12.92(4)	16.78(6)
$U^E/N\epsilon$	−0.907(1)	−1.033(1)	−1.012(1)	−1.126(1)	−1.272(1)	−1.471(1)	−1.739(1)	−2.119	−2.695
$T^* = 1.5$									
Z	9.32(2)	11.02(3)	8.81(2)	9.49(2)	10.54(2)	11.90(2)	13.89(3)	16.97(4)	23.19(4)
$U^E/N\epsilon$	−0.838(1)	−0.970(1)	−0.919(1)	−1.034(1)	−1.188	−1.393	−1.673	−2.070	−2.669
$T^* = 2.0$									
Z	9.65(2)	11.45(2)	9.22(2)	10.01(2)	11.21(2)	12.85(3)	15.28(2)	19.09(3)	26.46(4)
$U^E/N\epsilon$	−0.802	−0.930(1)	−0.877(1)	−0.992	−1.149	−1.357	−1.642	−2.047	−2.657
$T^* = 3.0$									
Z	10.03(2)	11.59(6)	9.56(2)	10.51(2)	11.89(2)	13.82(2)	16.66(2)	21.19(3)	29.87(4)
$U^E/N\epsilon$	−0.771	−0.883(3)	−0.838	−0.954	−1.112	−1.321	−1.611	−2.026	−2.647

[a] Corrections due to the truncation of the potential have not been included. The number between parentheses indicates the error in the last significant digit of the compressibility factor. For the excess energy, the statistical error in most cases is beyond the third decimal place and when this is the case, it is not indicated. [b] Averages over several independent runs.

of the perturbation theory (1) an "exact" first-order perturbation theory based on simulations performed on the reference hard-sphere fcc solid and (2) the Barker−Henderson perturbation theory. These two theories are compared in section IV with each other and with the simulation data reported in section II, and the concluding remarks are presented in the same section.

II. Monte Carlo Simulations for fcc Solids with Sutherland Potentials

We have performed NVT Monte Carlo simulations for fcc solids with potentials of the form in eq 1 with $\gamma = 6$, 12, 18, and 36, reduced temperatures $T^* = 0.2$, 0.4, 0.6, 0.8, 1.0, 1.5,

2.0, and 3.0, and reduced densities ρ^* in the range 0.90−1.30 with a step of 0.05, thus covering most of the density range for the solid and some of the high-density fluid. The potential cutoff distance was fixed at $r_c = 3\sigma$. Most of the systems consisted of $N = 500$ particles, but some simulations were carried out with 2048 particles to test the influence of the size of the system. The particles were placed in a cubic box with periodic boundary conditions in a fcc configuration. The system was equilibrated for 2×10^4 to 5×10^4 cycles, each cycle consisting of an attempted move per particle, and then the thermodynamic and structural properties were measured over the next 5×10^4 to 2×10^5 cycles, with 100 partial averages from which the statistical errors were determined as the standard deviation. The acceptance ratio was settled at around 50%. The excess energy U^E was determined from the energy equation in the form

$$\frac{U^E}{N} = 2\pi\rho\int_0^\infty g(r)r^2u(r)\mathrm{d}r \tag{2}$$

The compressibility factor Z was determined from the expression

$$Z = \frac{pV}{Nk_BT} = 1 + \frac{2}{3}\pi\rho\sigma^3 g(\sigma) + \frac{\gamma}{3}\epsilon\frac{U^E}{Nk_BT} \tag{3}$$

which results from the combination of eq 2 with the virial theorem for the Sutherland potential.

Results are listed in Tables 1−4, in which corrections to account for the effect of the truncation of the potential have not been included. For the Sutherland potential with a cutoff distance of $r_c = 3\sigma$, the corrections for the compressibility factor and the excess energy are

$$\Delta Z = \frac{2}{3}\pi\gamma\frac{3^{3-\gamma}}{3-\gamma}\frac{\rho^*}{T^*} \tag{4}$$

and

$$\frac{\Delta U^E}{N\epsilon} = 2\pi\frac{3^{3-\gamma}}{3-\gamma}\rho^* \tag{5}$$

respectively.

III. Perturbation Theory

In perturbation theories, the intermolecular potential is split in the form

$$u(r) = u_0(r) + u_1(r) \tag{6}$$

where $u_0(r)$ and $u_1(r)$ accounts essentially for the short-range and long-range contributions, respectively. The former is mainly due to the repulsive forces and the latter to the attractive ones. For the Sutherland potential (eq 1), the obvious choice for these contributions is

$$u_0(r) = \begin{cases} \infty & r \le \sigma \\ 0 & r > \sigma \end{cases} \tag{7}$$

and

$$u_1(r) = \begin{cases} 0 & r \le \sigma \\ -\epsilon\left(\frac{\sigma}{r}\right)^\gamma & r > \sigma \end{cases} \tag{8}$$

respectively. Note that eq 7 is the hard sphere (HS) potential.

At high densities, the thermodynamic and structural properties of a system are determined mainly by the first of these contributions, whence arise perturbation theories. These theories consider that the properties of the system at high densities are given by those of a reference system, one consisting of particles interacting by means of the potential $u_0(r)$ and providing the main contribution, plus a minor contribution due to $u_1(r)$ and considered as a perturbation of the former. As most of the thermodynamic systems with spherically symmetric potentials at high temperatures behave much like a hard-sphere system, the latter is the obvious choice for the reference system. Therefore, it is natural to express the thermodynamic properties as a series expansion in terms of $1/T^*$, the inverse of the reduced temperature, with the zero-order term corresponding to the contribution of the reference system and the remaining terms accounting for the contribution of the perturbation. In this situation, the Helmholtz free energy, the radial distribution function (rdf), the excess energy, and the compressibility factor can be expressed in the form

$$\frac{F}{Nk_BT} = \sum_{n=0}^{\infty}\frac{F_n}{Nk_BT}\frac{1}{T^{*n}} \tag{9}$$

$$g(r) = \sum_{n=0}^{\infty} g_n(r)\frac{1}{T^{*n}} \tag{10}$$

$$\frac{U^E}{N\epsilon} = \sum_{n=1}^{\infty}\frac{U_n}{N\epsilon}\frac{1}{T^{*n-1}} \tag{11}$$

and

$$Z = \sum_{n=0}^{\infty} Z_n\frac{1}{T^{*n}} \tag{12}$$

respectively, where subscripts "0" correspond to the contributions due to the reference system which, for systems with the Sutherland potential, is the hard-sphere system.

III. A. "Exact" First-Order Perturbation Theory. Before analysis of the performance of the Barker−Henderson perturbation theory for Sutherland solids, it is worth analyzing the capability of an "exact" perturbation theory for obtaining the thermodynamic properties of these solids. By "exact" we mean a perturbation theory with the terms in the expansions shown in eqs 10−12 obtained from computer simulations performed on the hard-sphere reference system, thus avoiding any theoretical approximation.

The procedure to determine the zero- and first-order terms in the expansion in eq 10 by means of computer simulation was developed by Smith et al.[22] quite a long time ago. They found

$$g_0\left(r_i + \frac{\Delta r}{2}\right) = \frac{3\langle N_i\rangle_0}{2\pi N\rho(r_{i+1}^3 - r_i^3)} \tag{13}$$

and

$$g_1\left(r_i + \frac{\Delta r}{2}\right) = -\frac{3\sum_j\{\langle N_iN_j\rangle_0 - \langle N_i\rangle_0\langle N_j\rangle_0\}u_1^*(r_j)}{2\pi N\rho(r_{i+1}^3 - r_i^3)} \tag{14}$$

In the preceding expressions, N_i is the number of intermolecular distances in the range (r_i, r_{i+1}), with $\Delta r = r_{i+1} - r_i \ll \sigma$, $i = 0$, 1, etc., angular brackets mean an average, the subscript 0 means

TABLE 5: Simulation Results for the First- and Second-Order Terms in Eq 20 for the Excess Energy and for the First-Order Term in Eq 21 for the Compressibility Factor[a]

ρ^*	0.90	0.95	1.00	1.05	1.10	1.15	1.20	1.25	1.30
$\gamma = 6$									
$U_1/N\epsilon$	−3.2887	−3.5046	−3.7975	−4.1182	−4.4604	−4.8219	−5.2044	−5.6101	−6.0390
$U_2/N\epsilon$	−0.0422	−0.0480	−0.0255	−0.0165	−0.0102	−0.0061	−0.0032	−0.0014	−0.0006
Z_1	−5.0394	−4.9246	−6.0803	−6.8668	−7.6766	−8.5003	−9.4207	−10.4063	−11.4665
$\gamma = 12$									
$U_1/N\epsilon$	−1.7926	−1.8739	−2.0831	−2.3401	−2.6416	−2.9926	−3.4009	−3.8762	−4.4301
$U_2/N\epsilon$	−0.1140	−0.1654	−0.1047	−0.0814	−0.0595	−0.0404	−0.0238	−0.0114	−0.0042
Z_1	−3.8516	−3.0405	−4.7486	−5.8621	−7.1573	−8.6718	−10.5498	−12.7860	−15.5226
$\gamma = 18$									
$U_1/N\epsilon$	−1.2963	−1.3173	−1.4750	−1.6842	−1.9449	−2.2679	−2.6699	−3.1737	−3.8097
$U_2/N\epsilon$	−0.1555	−0.2393	−0.1706	−0.1474	−0.1208	−0.0926	−0.0621	−0.0341	−0.0135
Z_1	−3.1964	−1.9759	−3.7698	−4.9272	−6.3832	−8.2302	−10.7525	−14.0598	−18.5391
$\gamma = 36$									
$U_1/N\epsilon$	−0.7178	−0.6889	−0.7684	−0.8861	−1.0448	−1.2603	−1.5602	−1.9919	−2.6386
$U_2/N\epsilon$	−0.1703	−0.2439	−0.2075	−0.2085	−0.2052	−0.1954	−0.1699	−0.1266	−0.0699
Z_1	−2.1226	−0.7260	−2.1174	−2.9374	−4.1180	−5.8108	−8.5834	−13.0358	−20.5802

[a] The zero-order term in the latter equation is accurately reproduced by the Hall equation (eq 27) for $\rho^* \geq 0.95$, and therefore it is not reported here.

that the averages are performed in the reference HS system, and $u_1^*(r) = u_1(r)/\epsilon$.

Introducing the rdf (eq 10), truncated at first order, into the energy equation (eq 2) provides the first- and second-order contributions to the excess energy in the form

$$U_1 = 2N\pi\rho\sum_i g_0(r_i) r_i^2 u_1(r_i)\Delta r \tag{15}$$

and

$$U_2 = 2N\pi\rho\sum_i g_1(r_i) r_i^2 u_1(r_i)\Delta r \tag{16}$$

respectively.

Introduction of the excess energy (eq 11), truncated at first order, into the virial equation of state (eq 3), provides the zero- and first-order contributions to the compressibility factor. They are

$$Z_0 = 1 + \frac{2}{3}\pi\rho\sigma^3 g_0(\sigma) \tag{17}$$

and

$$Z_1 = \frac{2}{3}\pi\rho\sigma^3 g_1(\sigma) + \frac{\gamma}{3}\epsilon\frac{U_1}{Nk_BT} \tag{18}$$

respectively.

In principle, the procedure might be generalized to obtain higher-order terms, but the computational effort increases with the order of the perturbative term and becomes impractical.

This procedure, that has been denoted Monte Carlo pertubation theory (MC-P),[25] was applied to obtain the first two terms in the perturbative expansions (eqs 10−12) for square-well fluids, first by Smith et al.[22] and more recently by two of us.[23−25] Very recently, we have successfully used the same procedure to obtain the thermodynamic and structural properties of fluids with the Sutherland potential.[11] To the best of our knowledge, the procedure has never been applied to crystalline solids.

The explicit expressions of eqs 10−12, truncated at the above-mentioned level, are as follows,

$$g(x) = g_0(x) + g_1(x)\frac{1}{T^*} \tag{19}$$

where $x = r/\sigma$ is the reduced distance,

$$\frac{U^E}{N\epsilon} = \frac{U_1}{N\epsilon} + \frac{U_2}{N\epsilon}\frac{1}{T^*} \tag{20}$$

and

$$Z = Z_0 + \frac{1}{T^*}Z_1 \tag{21}$$

We have performed Monte Carlo simulations in the NVT ensemble of the reference HS fluid to obtain the perturbative terms in the expressions in eqs 19−21. To this end, we considered a system consisting of 500 hard spheres placed in a fcc configuration within a cubic box with periodic boundary conditions. At each density, the system was allowed to equilibrate for 5×10^4 cycles and the averages involved in the expressions in eqs 13 and 14 were calculated from the next 10^6 cycles. We choose $\Delta r = 0.005$ and the acceptance ratio was set to about 50%. From these data, we have calculated the values of $g_0(x)$ and $g_1(x)$ from eqs 13 and 14, respectively, and subsequently U_1, U_2, Z_0, and Z_1 from eqs 15−18. The results for U_1, U_2, and Z_1 are listed in Table 5. The simulation data for Z_0, the compressibility factor of the hard-sphere solid, are accurately reproduced by eq 27 below, and therefore they have not been included in the table.

III. B. Barker−Henderson Perturbation Theory. The Barker−Henderson perturbation theory (BH) [18,19] provides expressions for the first- and second-order terms in the expansion in eq 9. The first-order term is given by

$$\frac{F_1}{Nk_BT} = 2\pi\rho\int_0^\infty u_1^*(r) g_0(r) r^2\,dr \tag{22}$$

The second-order term in the macroscopic compressibility approximation (mc) is

$$\frac{F_2}{Nk_BT} = -\pi\rho k_BT\int_0^\infty [u_1^*(r)]^2\left(\frac{\partial\rho}{\partial p}\right)_0 g_0(r) r^2\,dr \tag{23}$$

and in the local compressibility approximation (lc)

$$\frac{F_2}{Nk_BT} = -\pi\rho k_BT\int_0^\infty [u_1^*(r)]^2\left(\frac{\partial[\rho g_0(r)]}{\partial p}\right)_0 r^2\,dr \tag{24}$$

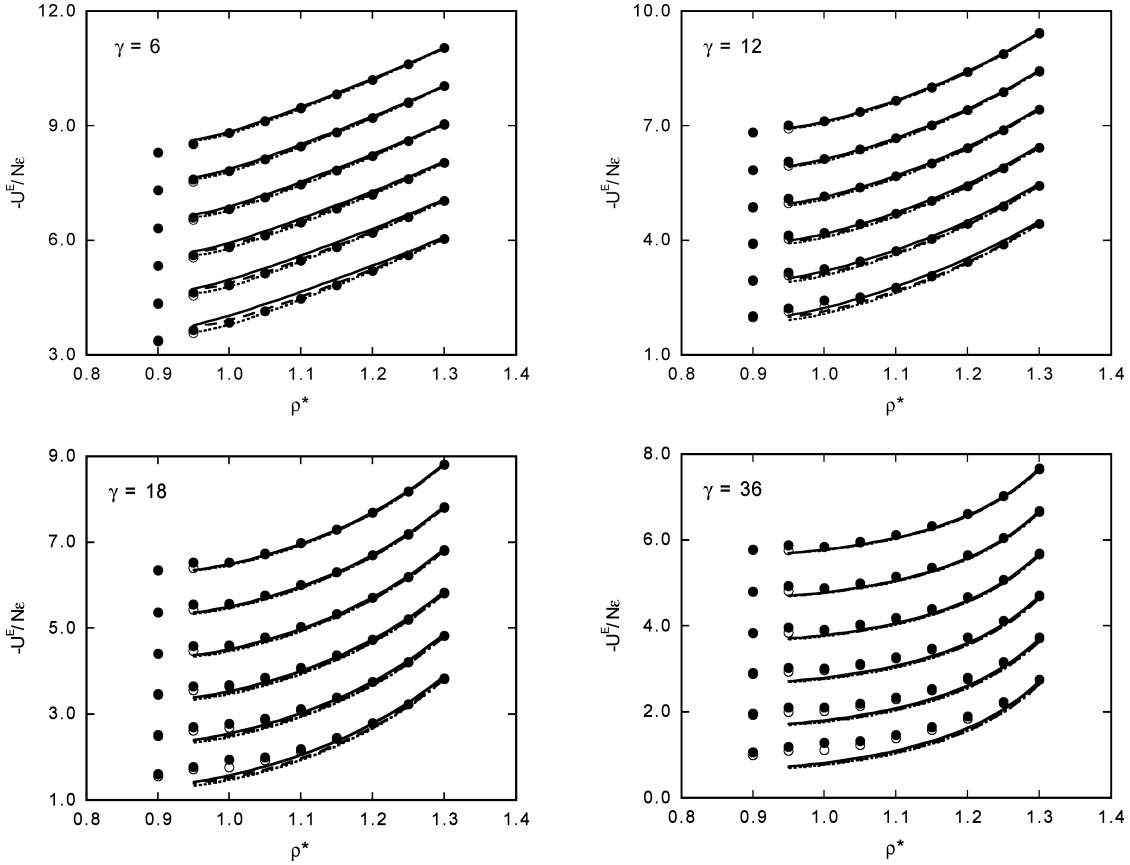

Figure 1. Comparison between MC simulations (●), from Tables 1−4, and perturbation theory for the excess energy $U^E/N\epsilon$ of Sutherland solids for $T^* = 0.6$, 0.8, 1.0, 1.5, 2.0, and 3.0 from the bottom upward. Open circles are the results from the MC perturbation theory as obtained from eq 20 with the data listed in Table 5. MC and MC-P results are indistinguishable from each other at the scale of the figure in most cases. Dotted curves are the results from the first-order Barker−Henderson perturbation theory, eqs 22 and 25. Dashed and continuous curves are the results from the second-order Barker−Henderson perturbation theory using the macroscopic and local compressibility approximations, eqs 23 and 24, respectively, together with eq 25. In most cases, the three curves are nearly indistinguishable from each other at the scale of the figure. For each temperature, the curves, and the corresponding sets of data, have been displaced upward for clarity by 1 unit with respect to those corresponding to the temperature immediately below.

The corresponding contributions to the excess energy can be readily obtained from the thermodynamic relationship

$$\frac{U^E}{N\epsilon} = -T^{*2}\left[\frac{\partial(F/Nk_BT)}{\partial T^*}\right]_V \tag{25}$$

and those for the compressibility factor from

$$Z_n = \frac{p_nV}{Nk_BT} = \rho\left[\frac{\partial(F_n/Nk_BT)}{\partial \rho}\right]_T \tag{26}$$

Using suitable expressions for the rdf $g_0(r)$ and the equation of state Z_0 of the HS reference fluid, Henderson and co-workers,[26−31] and many others, successfully applied the BH theory to a variety of model fluids.

The Barker−Henderson theory has been sometimes applied to crystalline solids.[14,32−34] To apply this theory, accurate expressions for the compressibility factor Z_0 and the rdf $g_0(r)$ of the hard-sphere reference fcc solid are needed. The equation of state of a fcc hard-sphere solid is well reproduced by the Hall[35] equation

$$Z_0 = 3/\alpha + 2.557696 + 0.1253077\beta + 0.1762393\beta^2 - 1.053308\beta^3 + 2.818621\beta^4 - 2.921934\beta^5 + 1.118413\beta^6 \tag{27}$$

where $\beta = 4\alpha/(1 + \alpha)$ and $\alpha = \rho_0/\rho - 1$, in which ρ_0 is the close-packing density.

In regard to the radial distribution function of the fcc hard-sphere solid, accurate parametrizations are available.[36−39] One of the most frequently used is[37]

$$g_0(x) = \frac{A}{x}\exp[-W_1{}^2(x - x_1)^2 - W_2{}^4(x - x_1)^4] + \frac{W}{24\eta\sqrt{\pi}}\sum_{i=2}^{\infty}\frac{n_i}{x_ix}\exp[-W^2(x - x_i)^2] \tag{28}$$

where $\eta = (\pi/6)\rho^*$ is the packing fraction and x_1 is the position of the first peak of the rdf, which was determined[36,37] from the simulation data for several packing fractions. Functions W_1, W_2, and W are given by,[40] for $\eta \le 0.55$,

$$W_1 = \sqrt{3}W_2 = \frac{\sqrt{3}}{0.50552}\exp[10.49375(\eta - 0.52)] \tag{29}$$

$$W = \frac{\sqrt{3}/2}{[0.23601(\eta - \eta_0)^2 - 21.4395(\eta - \eta_0)^5]^{1/2}} \tag{30}$$

For $0.55 < \eta \le 0.73$,

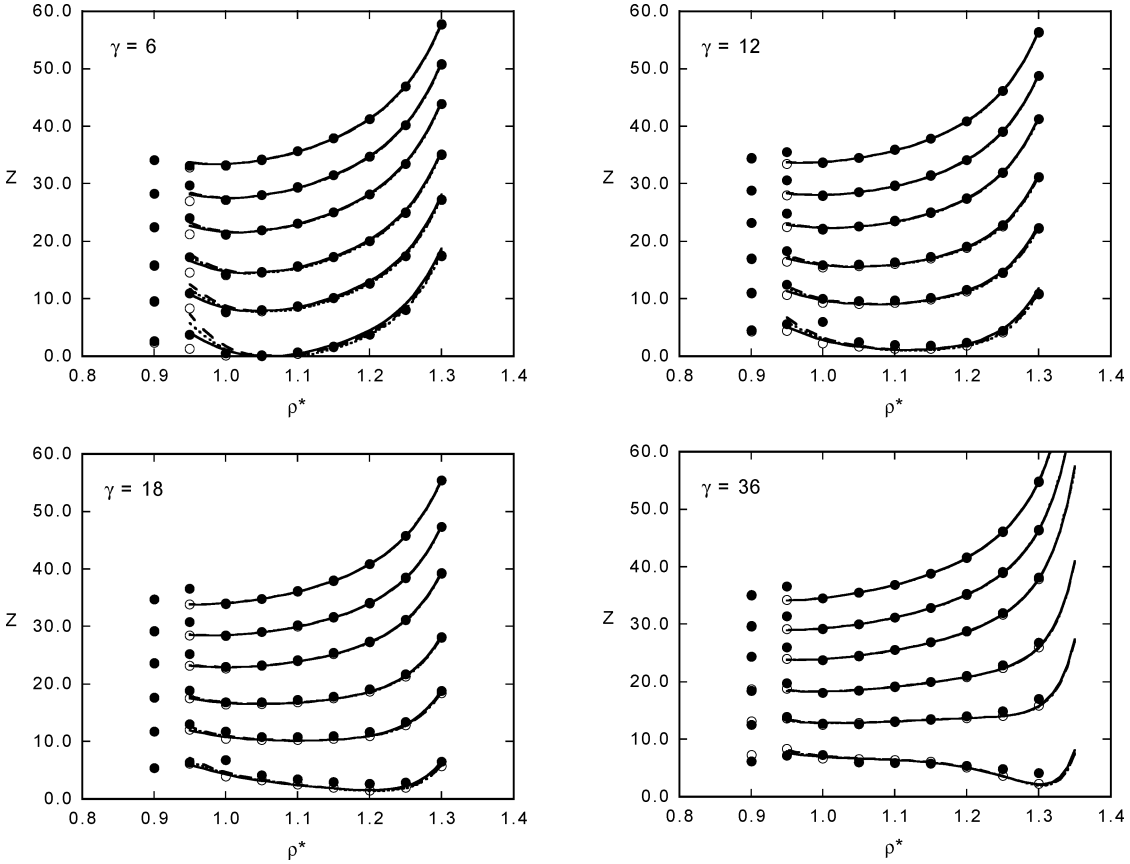

Figure 2. Comparison between MC simulations (●) and perturbation theory for the compressibility factor $Z = pV/Nk_BT$ of Sutherland solids for $T^* = 0.6$, 0.8, 1.0, 1.5, 2.0, and 3.0 from the bottom upward. Open circles are the results from the MC perturbation theory as obtained from eq 21 with the data listed in Table 5. Again, MC and MC-P results are nearly indistinguishable from each other. The curves have the same meaning as in Figure 1, with Z_1 and Z_2 obtained from eq 26. For each temperature, the curves, and the corresponding sets of data, have been displaced upward for clarity by 5 units with respect to those corresponding to the temperature immediately below.

$$W_1 = \frac{1.5522782}{\eta_0 - \eta} - 2.0302556 \exp[5.8331273(\eta_0 - \eta)] + 74.873192(\eta_0 - \eta)^2 \quad (31)$$

$$W_2 = \frac{0.9559565 - 5.855022(\eta_0 - \eta) + 39.74663(\eta_0 - \eta)^2 - 109.62638(\eta_0 - \eta)^3}{\eta_0 - \eta} \quad (32)$$

$$W = \frac{1 - 10.589574(\eta_0 - \eta)^{2.543}}{[0.694(\eta_0 - \eta)]^{1.072}} \quad (33)$$

In the preceding expressions, η_0 is the packing fraction corresponding to the close packing density ρ_0 for the fcc solid.

Finally, parameter A in the expression in eq 28 is determined from the condition that the virial theorem

$$Z_0 = 1 + 4\eta g_0 \quad (34)$$

must be satisfied.

Both the macroscopic and local compressibility approximations in the Barker−Henderson theory for the second-order term in the inverse-temperature series expansion of the Helmholtz free energy of fluids are known to give quite poor results, particularly for short-ranged potentials, and the same situation is expected to occur for crystalline solids. For fluids, a new procedure to obtain accurate estimates of the second- and higher-order terms in the pertubation expansion has been recently reported.[41,42] However, as this procedure is based on integral equation theory, it is not applicable to crystalline solids and we have to rely on the Barker−Henderson second-order perturbation theory.

IV. Results and Discussion

In Figure 1, the results for the excess energy from the BH and MC perturbation theories are compared with each other and with the MC simulation data for $T^* \geq 0.6$ listed in Tables 1−4, and a similar comparison is performed in Figure 2 for the compressibility factor. The upper limits in the integrals involved in the BH perturbation theory were set at $x = 3.0$, thus making possible a direct comparison with simulation data without the need of including in the latter the corrections due to the truncation of the potential. Let us first examine the MC simulation data. At densities $\rho^* \lesssim 0.95$, all the systems studied underwent a melting transition. Moreover, at the lowest temperatures considered, the transition showed a tendency, clearly seen in the figures, to displace toward higher densities ($\rho^* \approx 1.0$), and the effect is more pronounced the higher is the value of γ. This is a consequence of the clustering of the particles of these systems at low temperatures.

On the other hand, as we can see in the same tables, for $T^* = 0.4$ the compressibility factor is negative for part of the density range considered for all values of γ. This reveals that the systems are not in stable equilibrium for these densities. The same situation arises for $T^* = 0.2$ for the whole density range considered. Moreover, at the latter temperature and for intermediate densities, the structure of the systems reveals that they are highly defective fcc solids for all values of γ. In these

cases, simulation data are unreliable, and therefore they have not been included in the tables, because different runs lead to strongly different results, especially for the equation of state, which reveals that the system under simulation is failing to explore ergodically the configuration space.

Regarding the MC-P results for the excess energy U^E, one can see in Figure 1 that this "exact" first-order perturbation theory very accurately reproduces the simulation data for all the values of γ, at all temperatures $T^* \geq 0.6$ and densities except near melting at low temperatures. The same is true for the compressibility factor Z, as shown in Figure 2, except for $\gamma \geq 12$ and $T^* = 0.6$ and perhaps sometimes for $T^* = 0.8$ too. The reason for the better performance of the MC-P results for the excess energy than for the compressibility factor is, at least partially, because this "exact" perturbation theory is second order in the former quantity whereas it is only first order in the radial distribution function and the equation of state.

Now, let us analyze the performance of the BH perturbation theory. For the excess energy, at temperatures $T^* \geq 1.5$, the contribution of the second-order term is nearly negligible, so that the BH theory truncated at first-order provides satisfactory results in all cases for $T^* \geq 1.5$ and even for lower temperatures in the case with $\gamma = 6$. For $\gamma = 12$ and $T \leq 1.0$, second-order approximation is needed, with the local compressibility approximation providing greater accuracy than the macroscopic compressibility approximation. For $\gamma \geq 18$ and $T \leq 1.0$, the second-order approximation fails to provide completely satisfactory results for the low-density solid. It is to be remarked that even in the cases where the BH theory departs from simulation data, the "exact" first-order MC-P continues doing a good job.

As far as the equation of state is concerned, Figure 2 shows that the BH perturbation theory is in complete agreement with the MC-P theory up to densities close to the melting density, except perhaps for $\gamma \leq 18$ and $T^* = 0.6$, with little or no difference between first- and second-order approximations, although the local compressibility approximation seems to work slightly better at low temperatures than the first-order or the macroscopic compressibility approximations.

In Figures 1 and 2, we have not included the results for $T^* \leq 0.4$. For such low temperatures, the MC-P theory fails to accurately reproduce the simulation data for both the excess energy and the compressibility factor, as can be easily checked from the simulation data for the lower order terms in the expansions in eqs 11 and 12 listed in Table 5, using eqs 20 and 21, and comparing with the simulation data for $T^* = 0.4$ listed in Tables 1−4. Obviously, the performance of the BH perturbation theory at that temperature is still worse. To achieve enough accuracy from the MC-P theory at $T^* = 0.4$, higher order terms, determined from computer simulations, are needed in the expansions in eqs 11 nad 12. For still lower temperatures, say $T^* \lesssim 0.2$, even the NVT Monte Carlo simulations may not be reliable because the simulated system may not ergodically sample the phase space, as said before.

From the preceding analysis it seems clear that if we were capable of improving the theoretical predictions for the excess energy until the accuracy of the MC-P results was reached and the Helmholtz free energy route was used to obtain the equation of state instead of the pressure equation, the results obtained from the perturbation theory would probably be in complete agreement with the simulation data for the solids with spherically symmetrical potentials even for extremely short-ranged potentials and low temperatures. While this improvement is achieved, the Barker−Henderson perturbation theory constitutes an excellent choice in most situations. Alternatively, the MC-P theory can provide very reliable results, provided that simulation data for the quantities involved in eqs 20 and 21 are available, as in the present case where these quantities are listed in Table 5. Otherwise, the BH theory is advantageous as it requires less computational effort.

Acknowledgment. Financial support by the Spanish Ministerio de Ciencia y Tecnología (MCYT) under Grant No. BFM2003-001903 is acknowledged.

References and Notes

(1) Ben-Amotz, D.; Stell, G. *J. Chem. Phys.* **2003**, *119*, 10777−10788.
(2) Coutinho, J. A. P.; Vlamos, P. M.; Kontogeorgis, G. M. *Ind. Eng. Chem. Res.* **2000**, *39*, 3076−3082.
(3) Elvassore, N.; Prausnitz, J. M. *Fluid Phase Equilib.* **2002**, *194−197*, 567−577.
(4) Murakami, M. *J. Chem. Phys.* **2004**, *120*, 6751−6755.
(5) Zhang, Q.; Archer, L. A. *J. Chem. Phys.* **2004**, *121*, 10814−10824.
(6) Gil-Villegas, A.; Galindo, A.; Whitehead, P. J.; Mills, S. J.; Jackson, G. *J. Chem. Phys.* **1997**, *106*, 4166−4186.
(7) Davies, L. A.; Gil-Villegas, A.; Jackson, G. *Int. J. Thermophys.* **1998**, *19*, 675−686.
(8) Wu, J.; Huang, G.; Hu, Z. *Macromolecules* **2003**, *36*, 440−448.
(9) Paricaud, P. *J. Chem. Phys.* **2006**, *124*, 154505-1−154505-17.
(10) Heyes, D. M.; Woodcock, L. V. *Mol. Phys.* **1986**, *59*, 1369−1388.
(11) Díez, A.; Largo, J.; Solana, J. R. *J. Chem. Phys.* **2006**, *125*, 074509-1−074509-12.
(12) Díez, A.; Largo, J.; Solana, J. R. *Fluid Phase Equilib.* **2007**, 67−73.
(13) Camp, P. J.; Patey, G. N. *J. Chem. Phys.* **2001**, *114*, 399−408.
(14) Camp, P. J. *Phys. Rev. E* **2003**, *67*, 011503-1−011503-8.
(15) Kurochkin, V. I. *Sov. Phys. Lebedev Inst. Rep. (U.S.A.)* **1990**, *8*, 1−2.
(16) Largo, J.; Solana, J. R. *Int. J. Thermophys.* **2000**, *21*, 899−908.
(17) Jiuxun, S. *Can. J. Phys.* **2005**, *83*, 55−66.
(18) Barker, J. A.; Henderson, D. *J. Chem. Phys.* **1967**, *47*, 2856−2861.
(19) Barker, J. A.; Henderson, D. *Annu. Rev. Phys. Chem.* **1972**, *23*, 439−484.
(20) Tang, Y.; Lu, B. C.-Y. *J. Chem. Phys.* **1993**, *99*, 9828−9835.
(21) Tang, Y.; Lu, B. C.-Y. *Mol. Phys.* **1997**, *90*, 215−224.
(22) Smith, W. R.; Henderson, D.; Barker, J. A. *J. Chem. Phys.* **1971**, *55*, 4027−4033.
(23) Largo, J.; Solana, J. R. *Mol. Simul.* **2003**, *29*, 363−371.
(24) Largo, J.; Solana, J. R. *Fluid Phase Equilib.* **2003**, *212*, 11−29.
(25) Largo, J.; Solana, J. R. *J. Phys. Chem. B* **2004**, *108*, 10062−10070.
(26) Barker, J. A.; Henderson, D. *J. Chem. Phys.* **1967**, *47*, 4714−4721.
(27) Barker, J. A.; Henderson, D. *4th Symp. Thermophys. Prop.* **1968**, 30−36.
(28) Smith, W. R.; Henderson, D.; Barker, J. A. *Can. J. Phys.* **1968**, *46*, 1725−1727.
(29) Smith, W. R.; Henderson, D.; Barker, J. A. *J. Chem. Phys.* **1970**, *53*, 508−515.
(30) Smith, W. R.; Henderson, D.; Barker, J. A. *Can. J. Phys.* **1975**, *53*, 5−12.
(31) Henderson, D.; Scalise, O. H.; Smith, W. R. *J. Chem. Phys.* **1980**, *72*, 2431−2438.
(32) Tavares, F. W.; Sandler, S. I. *AIChE J.* **1997**, *43*, 219−231.
(33) Tavares, F. W.; Prausnitz, J. M. *Colloid Polym. Sci.* **2004**, *282*, 620−632.
(34) Zhou, S. *J. Phys. Chem. B* **2004**, *108*, 8447−8451.
(35) Hall, K. R. *J. Chem. Phys.* **1972**, *57*, 2252−2254.
(36) Weis, J.-J. *Mol. Phys.* **1974**, *28*, 187−195. Ibid: Weis, J.-J. *Mol. Phys.* **1976**, *32*, 296.
(37) Kincaid, J. M.; Weis, J. J. *Mol. Phys.* **1977**, *34*, 931−938.
(38) Rascón, C.; Mederos, L.; Navascués, G. *J. Chem. Phys.* **1996**, *105*, 10527−10534.
(39) Velasco, E.; Mederos, L.; Navascués, G. *Mol. Phys.* **1999**, *97*, 1273−1277.
(40) Kang, H. S.; Ree, T.; Ree, F. H. *J. Chem. Phys.* **1986**, *84*, 4547−4557.
(41) Zhou, S. *J. Chem. Phys.* **2006**, *125*, 144518-1−144518-7.
(42) Zhou, S. *Phys. Rev. E* **2006**, *74*, 031119-1−031119-7.